

Evaluation of Backbone Proton Positions and Dynamics in a Small Protein by Liquid Crystal NMR Spectroscopy

Tobias S. Ulmer, Benjamin E. Ramirez,[†] Frank Delaglio, and Ad Bax*

Contribution from the Laboratory of Chemical Physics, National Institute of Diabetes and Digestive and Kidney Diseases, National Institutes of Health, Bethesda, Maryland 20892

Received March 9, 2003; E-mail: bax@nih.gov

Abstract: NMR measurements of a large set of protein backbone one-bond dipolar couplings have been carried out to refine the structure of the third IgG-binding domain of Protein G (GB3), previously solved by X-ray crystallography at a resolution of 1.1 Å. Besides the commonly used bicelle, poly(ethylene glycol), and filamentous phage liquid crystalline media, dipolar couplings were also measured when the protein was aligned inside either positively or negatively charged stretched acrylamide gels. Refinement of the GB3 crystal structure against the $^{13}\text{C}^\alpha\text{--}^{13}\text{C}'$ and $^{13}\text{C}'\text{--}^{15}\text{N}$ dipolar couplings improves the agreement between experimental and predicted $^{15}\text{N}\text{--}^1\text{H}^\text{N}$ as well as $^{13}\text{C}^\alpha\text{--}^1\text{H}^\alpha$ dipolar couplings. Evaluation of the peptide bond N–H orientations shows a weak anticorrelation between the deviation of the peptide bond torsion angle ω from 180° and the angle between the N–H vector and the C'–N–C $^\alpha$ plane. The slope of this correlation is –1, indicating that, on average, pyramidalization of the peptide N contributes to small deviations from peptide bond planarity ($\langle\omega\rangle = 179.3 \pm 3.1^\circ$) to the same degree as true twisting around the C'–N bond. Although hydrogens are commonly built onto crystal structures assuming the N–H vector orientation falls on the line bisecting the C'–N–C $^\alpha$ angle, a better approximation adjusts the C $^\alpha$ –C'–N–H torsion angle to –2°. The $^{15}\text{N}\text{--}^1\text{H}^\text{N}$ dipolar data do not contradict the commonly accepted motional model where angular fluctuations of the N–H bond orthogonal to the peptide plane are larger than in-plane motions, but the amplitude of angular fluctuations orthogonal the C $^\alpha$ _{i-1}–N_i–C $^\alpha$ _i plane exceeds that of in-plane motions by at most 10–15°. Dipolar coupling analysis indicates that for most of the GB3 backbone, the amide order parameters, *S*, are highly homogeneous and vary by less than ±7%. Evaluation of the H $^\alpha$ proton positions indicates that the average C $^\alpha$ –H $^\alpha$ vector orientation deviates by less than 1° from the direction that makes ideal tetrahedral angles with the C $^\alpha$ –C $^\beta$ and C $^\alpha$ –N vectors.

Introduction

Traditionally, structure determination of proteins by NMR has relied mostly on the use of interproton distance restraints, derived from NOEs, and torsion angle restraints, derived from *J* couplings.^{1,2} The vast majority of these restraints involve hydrogen nuclei, and the positions of the carbon, nitrogen, and oxygen atoms in the final structure are generally derived in an indirect manner, using standard knowledge about bond lengths and angles and the planarity of peptide groups. More recently, these parameters have become supplemented by heteronuclear dipolar couplings, which restrain the orientation of internuclear vectors relative to the protein's alignment frame when immersed in an aligning, usually liquid crystalline medium.^{3,4} In X-ray crystallography, the inverse usually applies: the carbon, nitro-

gen, and oxygen atoms contribute most to the X-ray diffraction patterns, and in favorable cases, high-resolution structures can be solved without imposing knowledge about bond lengths and angles.⁵ However, hydrogen electron density is usually too weak to permit accurate determination of proton positions in proteins. Protons typically are added computationally, using knowledge of the bond length, and assuming planar or tetrahedral geometry.⁶ So, neither conventional NMR structures nor X-ray structures provide independent quantitative information on the position of hydrogens relative to the carbon/nitrogen framework in proteins.

Accurate knowledge of the position of hydrogen atoms relative to the backbone framework is important not only to improve the accuracy of structures determined from dipolar coupling and NOE data but also to understanding and calibrating the various intramolecular forces. For example, little is known about how the position of protein amide hydrogens relative to the backbone is affected by regular, weak hydrogen bonds. Commonly, in NMR structure determination, the amide proton

* Corresponding author: Building 5, Room 126, NIH, Bethesda, MD 20892-0520. Phone: 301 496 2848. Fax: 301 402 0907.

[†] Present address: Department of Chemistry, Northwestern University, Evanston, IL 60208-3113.

(1) Wüthrich, K. *NMR of Proteins and Nucleic Acids*; John Wiley & Sons: New York, 1986.

(2) Clore, G. M.; Gronenborn, A. M. *Crit. Rev. Biochem. Mol. Biol.* **1989**, *24*, 479–564.

(3) Tjandra, N.; Bax, A. *Science* **1997**, *278*, 1111–1114.

(4) Prestegard, J. H. *Nat. Struct. Biol.* **1998**, *5*, 517–522.

(5) Perutz, M. *Protein Structure – New Approaches to Disease and Therapy*; W. H. Freeman: New York, 1992.

(6) Brunger, A. T. *XPLOR: A System for X-ray Crystallography and NMR*, ed. 3.1; Yale University Press: New Haven, 1993.

is assumed to be located on the line that bisects the $C'-N-C^\alpha$ angle, and peptide bond planarity is enforced because experimental NMR parameters contain insufficient information to improve on this assumption.⁶ In contrast, considerable deviations from planarity of the peptide bond ($\omega = 180^\circ$) can be identified in atomic resolution X-ray structures, sometimes exceeding $10-15^\circ$.^{7,8} Theoretical calculations optimizing the geometry of unsolvated, non-hydrogen-bonded dipeptide models are indicative of considerable pyramidalization at the peptide N, such that the N-H vector makes a significant angle of ca. 15° with the $C'-N-C^\alpha$ plane.^{9,10} Similarly, $^{13}C'$ chemical shift calculations in α -helices have been reported to agree only with experimental shifts if considerable pyramidalization of the amide moiety is invoked.¹¹ In contrast, in β -sheets, agreement was satisfactory without requiring such pyramidalization.¹¹ However, a previous NMR study of the amide proton positions, which relied on measurement of the six 3J couplings between H^N/C' and H^α , C^β , and C' , contrasted with the computational results and indicated that the N-H vector makes an angle with the $C'-N-C^\alpha$ plane that has a root-mean-square (rms) value considerably less than 8° , with no significant dependence of this angle on secondary structure discernible.¹²

For the C^α site, details of the local geometry are a function of the backbone torsion angles and bond angles. In particular, the $N-C^\alpha-C'$ angle, τ_3 , can differ substantially from the ideal tetrahedral value of 109.4° .¹³ However, relatively little is known about precisely where the H^α proton is situated relative to the other C^α substituents and whether this position depends on secondary structure, residue type, or χ_1 angle.

The current study utilizes heteronuclear one-bond dipolar couplings between amide ^{15}N and $^1H^N$, $^1D_{NH}$, and between $^{13}C^\alpha$ and $^1H^\alpha$, $^1D_{C^\alpha H^\alpha}$, to define the orientation of the N-H and $C^\alpha-H^\alpha$ vectors relative to the protein backbone for the 56-residue third IgG-binding domain of Protein G (GB3). $^1D_{NH}$ and $^1D_{C^\alpha H^\alpha}$ dipolar couplings can be readily measured at high accuracy in proteins that are weakly aligned with respect to the magnetic field, either by their own magnetic susceptibility anisotropy,^{14,15} by a dilute liquid crystalline medium,^{3,16,17} or by an anisotropically compressed gel matrix.¹⁸⁻²⁰ These one-bond couplings are very precise monitors of the time-averaged orientation of the corresponding bond vectors relative to the external magnetic field. Provided the orientation of the protein's backbone framework relative to the magnetic field is known accurately,

the dipolar couplings thereby define the orientation of the N-H and C-H vectors relative to this framework. By using a variety of alignment media, the measurement of dipolar couplings can be repeated at different average orientations of the protein relative to the magnetic field, removing the degeneracy existing when a single alignment medium is used.^{21,22}

For the GB3 domain, a 1.1 \AA resolution X-ray crystal structure²³ provides the coordinates of the heavy atoms. In addition to the measurement of $^1D_{NH}$ and $^1D_{C^\alpha H^\alpha}$ couplings in five different alignment media, the $^1D_{C'N}$ and $^1D_{C'C^\alpha}$ backbone couplings were measured. When using these latter couplings to refine the X-ray structure, a modest improvement in structural quality was obtained, as evaluated by cross-validation. Even though the backbone atomic positions in this refined structure differ by only 0.3 \AA from the original X-ray structure, we show that the $^{15}N-H$ and $^{13}C^\alpha-H^\alpha$ vector orientations relative to this refined backbone are, on average, closer to their standard orientations than when using the original X-ray structure.

Experimental Section

NMR Sample Preparation. GB3 was overexpressed in *Escherichia coli* HMS174, using uniformly ^{13}C -enriched glucose and $^{15}NH_4Cl$ in M9 minimal medium.²⁴ Six GB3 samples, termed A-F, were prepared. Each sample contained 0.2 mg/mL NaN_3 , 8% D_2O , and GB3 at a concentration of $\sim 1.5 \text{ mM}$. In addition, sample A contained 4.2% bicelles (w/v), composed of ditetradecyl-phosphatidylcholine and dihexyl-phosphatidylcholine in a molar ratio of $3:1$,²⁵ as well as cetyltrimethylammonium bromide (CTAB) in a molar ratio of $1:30$ versus ditetradecyl-phosphatidylcholine,²⁶ in 20 mM imidazole, 25 mM NaH_2PO_4/Na_2HPO_4 , pH 6.5 aqueous solution. Sample B contained C12E5 alkyl poly(ethylene glycol) and *n*-hexanol in 25 mM NaH_2PO_4/Na_2HPO_4 pH 6.5 solution. The C12E5 surfactant-to-water ratio was 4.3% (w/v), and the molar ratio of surfactant/alcohol was 0.96 .²⁷ Sample C contained 11 mg/mL Pf1 phage, strain LP11-92 (ASLA, Ltd., Latvia) in 100 mM $NaCl$, 25 mM NaH_2PO_4/Na_2HPO_4 , pH 6.5 solution.¹⁶ Samples D and E contained axially stretched¹⁸⁻²⁰ negatively and positively charged polyacrylamide gels, respectively, prepared as described below. Sample F was in isotropic aqueous solution.

Charged Polyacrylamide Gels. Gels were polymerized from a solution of 6.3% (w/v) acrylamide/bisacrylamide ($39:1$ w/w), 0.11% (w/v) ammoniumperoxide sulfate, 0.37% (v/v) N,N,N',N' -tetramethylethylenediamine (TEMED) in 100 mM Tris/HCl pH 8.1. To introduce negative charges, 5% acrylamide (AA) was replaced by an equimolar amount of 2-acrylamido-2-methyl-1-propanesulfonic acid (AMPS, Sigma-Aldrich, Inc.). To introduce positive charges, 5% acrylamide was replaced by 10 times the equimolar amount of diallyldimethylammonium chloride (DADMAC; Sigma-Aldrich, Inc.). The 10-fold excess²⁸ was used to compensate for the slower rate of DADMAC polymerization relative to that of AA. After addition of all components to a final volume of $270 \mu\text{L}$, $255 \mu\text{L}$ was immediately transferred to a cylinder of 5.4 mm diameter and allowed to polymerize overnight. Polymerized gels were first equilibrated overnight in 50 mL 100 mM NaH_2PO_4/Na_2HPO_4 pH 6.8, followed by immersion in 50 mL of H_2O for 16 h. Subsequently, the gels were dehydrated at 37°C to a volume of about $20-30 \mu\text{L}$, prior to soaking for 36 h in a $255 \mu\text{L}$ of protein

- (7) Wlodawer, A.; Walter, J.; Huber, R.; Sjolin, L. *J. Mol. Biol.* **1984**, *180*, 301-329.
- (8) MacArthur, M. W.; Thornton, J. M. *J. Mol. Biol.* **1996**, *264*, 1180-1195.
- (9) Head-Gordon, T.; Head-Gordon, M.; Frisch, M. J.; Brooks, C. L.; Pople, J. A. *J. Am. Chem. Soc.* **1991**, *113*, 5989-5997.
- (10) Edison, A. S.; Weinhold, F.; Westler, W. M.; Markley, J. L. *J. Biomol. NMR* **1994**, *4*, 543-551.
- (11) Sulzbach, H. M.; Schleyer, P. v. R.; Schaefer, H. F. *J. Am. Chem. Soc.* **1995**, *117*, 2632-2637.
- (12) Hu, J. S.; Bax, A. *J. Am. Chem. Soc.* **1997**, *119*, 6360-6368.
- (13) Karplus, P. A. *Prot. Sci.* **1996**, *5*, 1406-1420.
- (14) Gayathri, C.; Bothnerby, A. A.; Vanzijl, P. C. M.; Maclean, C. *Chem. Phys. Lett.* **1982**, *87*, 192-196.
- (15) Tolman, J. R.; Flanagan, J. M.; Kennedy, M. A.; Prestegard, J. H. *Proc. Natl. Acad. Sci. U.S.A.* **1995**, *92*, 9279-9283.
- (16) Hansen, M. R.; Mueller, L.; Pardi, A. *Nature Struct. Biol.* **1998**, *5*, 1065-1074.
- (17) Clore, G. M.; Starich, M. R.; Gronenborn, A. M. *J. Am. Chem. Soc.* **1998**, *120*, 10571-10572.
- (18) Tycko, R.; Blanco, F. J.; Ishii, Y. *J. Am. Chem. Soc.* **2000**, *122*, 9340-9341.
- (19) Sass, H. J.; Musco, G.; Stahl, S. J.; Wingfield, P. T.; Grzesiek, S. *J. Biomol. NMR* **2000**, *18*, 303-309.
- (20) Chou, J. J.; Gaemers, S.; Howder, B.; Louis, J. M.; Bax, A. *J. Biomol. NMR* **2001**, *21*, 377-382.

- (21) Ramirez, B. E.; Bax, A. *J. Am. Chem. Soc.* **1998**, *120*, 9106-9107.
- (22) Al-Hashimi, H. M.; Valafar, H.; Terrell, M.; Zartler, E. R.; Eidsness, M. K.; Prestegard, J. H. *J. Magn. Reson.* **2000**, *143*, 402-406.
- (23) Derrick, J. P.; Wigley, D. B. *J. Mol. Biol.* **1994**, *243*, 906-918.
- (24) Sambrook, J.; Fritsch, E. F.; Maniatis, T. *Molecular Cloning, a Laboratory Manual*; Cold Spring Harbor Laboratory Press: Plainview, NY, 1989.
- (25) Otting, M.; Bax, A. *J. Biomol. NMR* **1999**, *13*, 187-191.
- (26) Losonczi, J. A.; Prestegard, J. H. *J. Biomol. NMR* **1998**, *12*, 447-451.
- (27) Ruckert, M.; Otting, G. *J. Am. Chem. Soc.* **2000**, *122*, 7793-7797.
- (28) Vegvari, A.; Foldesi, A.; Hetenyi, C.; Kocnegarova, O.; Schmid, M. G.; Kudirkaite, V.; Hjerten, S. *Electrophoresis* **2000**, *21*, 3116-3125.

solution composed of 92% H₂O, 8% D₂O, and 45 mM NaH₂PO₄/Na₂HPO₄, pH 6.5, containing 0.02% NaN₃ (w/v). Gels were taken up in a cylinder 6.0 mm in diameter and forced into an open-ended NMR tube (New Era Enterprises, Inc.) through a connecting funnel, as described previously.²⁰ For easier passage into the NMR tube, a small amount of buffer (~20 μL) was used as a lubricant. The NMR tube was sealed with an O-ring-containing plug at the bottom and a Shigemitsu plunger on top.²⁰ Following a 3 day equilibration period in the NMR tube, no changes in solvent ²H quadrupolar splitting (4.35 and 3.15 Hz for the negatively and positively charged gels, respectively) were detected over a period of several months, and the osmotic pressure of the charged gel²⁹ prevented the slow contraction commonly seen in compressed neutral gels.

NMR Spectroscopy. NMR spectra were recorded on Bruker DMX600, DMX750, and DRX800 spectrometers equipped with triple-resonance, three-axes pulsed field gradient probeheads. Data for sample B were collected at 31 °C, for samples A and C at 29 °C, and for samples D–F at 25 °C. Slightly different sample temperatures were chosen in order to optimize the stability of the degree of alignment for each sample over the data collection period of multiple days. Protein G is extremely stable, with a melting temperature above 60 °C, and the absence of significant changes in chemical shifts over the 25–31 °C temperature range indicates the absence of detectable changes in structure or dynamics. C^α–C', C^α–H^α, and N–H dipolar couplings were derived from the difference in splittings between the aligned (samples A–E) and isotropic states (sample F). One-bond ¹⁵N–¹H splittings were extracted from two-dimensional IPAP [¹⁵N,¹H]-HSQC spectra,³⁰ recorded with acquisition times of 128 ms (¹⁵N) and 83 ms (¹H) as two interleaved data matrices, each consisting of 256 × 768 complex points. ¹D_{CaHa} values were obtained from three-dimensional CT-(H)CA(CO)NH experiments³¹ using acquisition times of 25.3 (¹³C^α), 27.5 (¹⁵N), and 54.8 ms (¹H) and data matrices of 64 × 36 × 512 complex points. ¹D_{CaC'} values were obtained from ¹³C^α-coupled three-dimensional HNCO spectra, recorded at 150.9 MHz ¹³C frequency, with acquisition times of 144 (¹³C), 24 (¹⁵N), and 59 ms (¹H), using data matrices consisting of 225 × 16 × 512 complex points. ¹D_{CN} dipolar couplings were determined from the amplitude ratios in quantitative *J*-correlation TROSY-HNCO experiments.³² These HNCO data matrices consisted of 40 × 48 × 512 complex points, with acquisition times of 28 (¹³C'), 55 (¹⁵N), and 57 ms (¹H).

Spectra were processed and analyzed with the NMRPipe package.³³ Sine-bell and squared sine-bell windows functions, typically shifted by 72° and truncated at 176°, were applied in the indirectly and directly detected dimensions, respectively. Data were extensively zero-filled prior to Fourier transformation, to yield high digital resolution. Errors in extracted dipolar couplings were estimated to be 0.10 Hz for C'–N, 0.10 Hz for C^α–C', 0.58 Hz for C^α–H^α, and 0.26 Hz for N–H couplings.

Structure Refinement. Simulated annealing calculations were carried out with the program DYNAMO 2.1.³⁴ The standard force field terms (atoms, angles, bonds, impropers, van der Waals) were operative. As described below, atomic coordinate (AC) restraints were used that force the local structure to mimic the 1.1 Å crystal structure. In addition to the dipolar coupling (DC) restraints, 34 experimentally validated hydrogen bonds³⁵ were defined. The force constant for each energy term was optimized to yield optimal cross-validation^{36–38} of the obtained structures. Values used are included as Supporting Information Table 1.

The AC restraints were incorporated by defining overlapping three-residue fragments of GB3, each fragment shifted by one residue, utilizing the Protein Data Bank 1IGD coordinates of GB3. The AC restraints aim to minimize the backbone rmsd between each X-ray structure fragment and its corresponding fragment in the final structure. Use of these short fragments permits only small changes in the local structure but allows moderate changes in the global structure of the protein.

For the DC restraints, all one-bond dipolar couplings obtained in a given medium (A–E) were described by a single alignment tensor, using previously reported effective internuclear distances for appropriate scaling relative to the ¹⁵N–¹H interaction³⁹ and assuming a uniform order parameter *S* for each type of interaction. Differences in *S* for different types of interactions are already taken into account by using the vibrationally corrected, effective internuclear distances, calibrated previously.⁴⁰ To compensate for the different strength of alignment between different media, tensor-specific force constants, proportional to the inverse of the square of the respective alignment tensor magnitudes, *D_a*, were introduced, so that each medium contributed comparably to the overall DC energy term. Additionally, the force constants were adjusted to the square of the inverse error in the experimental measurement, resulting in relative magnitudes of the force constants for the C^α–C', C'–N, C^α–H^α, and N–H couplings of 100:100:13:3.

Simulated annealing (SA) comprised an initialization period of 200 time steps of 3 fs at 500 K, followed by cooling to 0 K in 3000 steps of 5 fs. To balance the force constants between the different energy terms, initially only C^α–C' and C'–N couplings were included in the DC restraint list. In this case, the H^N and H^α atoms were deleted after each structure calculation and reintroduced at their standard positions (H^N is placed on a line that bisects the C'_{*i*}–N_{*i*+1}–C^α_{*i*+1} angle, and the H^α proton is placed such that the H^α–C^α vector makes 109.4° angles with the N–C^α and C^α–C^β bonds). If the backbone heavy-atom positions improve, an improved agreement with the C^α–H^α and N–H dipolar couplings may then be expected, compared to the X-ray structure, as some of the deviations of H^N and H^α from their standard positions are caused by the random error in heavy-atom backbone coordinates present in the X-ray structure. It is also noted that during SA runs without C^α–H^α and N–H couplings, no DC restraints act directly on H^N and H^α, and in none of the SA runs is there a direct DC restraint affecting C^β, whose position is critical when reinserting the H^α atom. Additionally, an AC restraint acts on C^β. Considering this, improved H^N cross-validation was obtained by relaxing the peptide planarity restraint somewhat (by reducing the H^N–N–C'–C^α improper force constant 10-fold relative to the other improper terms) and improved H^α cross-validation was obtained when strengthening the tetrahedral arrangement around the C^α atom (by increasing the force constants for the angular terms H^α–C^α–C^β, N–C^α–C^β and improper term H^α–N–C'–C^β 4-fold relative to the other angular and improper terms, respectively) in order to transfer the C^α–C' and C'–N DC restraints more efficiently to the C^β position. These modifications were found to be less important if the C^α–H^α and/or N–H dipolar couplings were included in the SA runs (where the obtained H^α and/or H^N position are retained at the end of the calculation, as in regular NMR structure calculations) but, for consistency, were kept the same in all SA runs.

Four different GB3 structures, refined in the manner defined above, were calculated. Refined-I was calculated by including the C^α–C' and C'–N dipolar coupling restraints. Refined-II was calculated by including all four types of dipolar coupling restraints. Refined-III was calculated by including the C^α–C', C'–N, and C^α–H^α dipolar restraints. Refined-IV was calculated by including the C^α–C', C'–N, and N–H dipolar

- (29) Horkay, F.; Tasaki, I.; Bassar, P. J. *Biomacromolecules* **2000**, *1*, 84–90.
 (30) Ottiger, M.; Delaglio, F.; Bax, A. *J. Magn. Reson.* **1998**, *131*, 373–378.
 (31) Tjandra, N.; Bax, A. *J. Am. Chem. Soc.* **1997**, *119*, 9576–9577.
 (32) Chou, J. J.; Delaglio, F.; Bax, A. *J. Biomol. NMR* **2000**, *18*, 101–105.
 (33) Delaglio, F.; Grzesiek, S.; Vuister, G. W.; Zhu, G.; Pfeifer, J.; Bax, A. *J. Biomol. NMR* **1995**, *6*, 277–293.
 (34) Delaglio, F. *Dynamo NMR Molecular Structure Engine Version 2.1*. <http://spin.niddk.nih.gov/NMRPipe/dynamo/> (accessed 2002).
 (35) Cornilescu, G.; Ramirez, B. E.; Frank, M. K.; Clore, G. M.; Gronenborn, A. M.; Bax, A. *J. Am. Chem. Soc.* **1999**, *121*, 6275–6279.
 (36) Cornilescu, G.; Marquardt, J. L.; Ottiger, M.; Bax, A. *J. Am. Chem. Soc.* **1998**, *120*, 6836–6837.

- (37) Drohat, A. C.; Tjandra, N.; Baldissari, D. M.; Weber, D. J. *Prot. Sci.* **1999**, *8*, 800–809.
 (38) Clore, G. M.; Garrett, D. S. *J. Am. Chem. Soc.* **1999**, *121*, 9008–9012.
 (39) Cornilescu, G.; Bax, A. *J. Am. Chem. Soc.* **2000**, *122*, 10143–10154.
 (40) Ottiger, M.; Bax, A. *J. Am. Chem. Soc.* **1998**, *120*, 12334–12341.

Table 1. Normalized Scalar Products between the Alignment Tensors Obtained for GB3 in Aligning Media A–E, Calculated Using the GB3 Crystal Structure (1IGD)

medium ^a	A	B	C	D	E
A	1	0.796	-0.404	0.315	0.873
B		1	-0.606	0.224	0.594
C			1	0.633	-0.606
D				1	-0.132
E					1

^a Key: A, bicelle; B, PEG; C, Pf1 phage; D and E, negatively and positively charged polyacrylamide gels, respectively.

Table 2. Agreement between Various GB3 Structures and Experimental Dipolar Couplings

coupling ^a	structure ^b	Q _A ^c	Q _B	Q _C	Q _D	Q _E	Q _{avg}	rmsd _{av} ^d
C ^α –C'	crystal	16.1	17.3	12.9	12.4	14.3	14.6	0.29 ± 0.15
	refined-I	9.1	9.2	7.9	7.6	8.5	8.5	0.18 ± 0.07
	refined-II	9.3	9.5	8.0	6.7	8.3	8.4	0.17 ± 0.07
C'–N	crystal	24.8	21.2	20.3	14.2	30.3	22.2	0.21 ± 0.18
	refined-I	9.6	12.9	11.0	9.2	13.5	11.2	0.13 ± 0.07
	refined-II	9.3	12.9	10.4	8.6	13.7	11.0	0.12 ± 0.07
C ^α –H ^α	crystal	12.1	9.3	12.0	16.3	11.0	12.1	1.99 ± 1.21
	refined-I	11.0	8.6	10.8	14.3	10.3	11.0	1.83 ± 1.11
	refined-II	2.2	2.1	2.5	2.2	2.1	2.2	0.40 ± 0.19
N–H	crystal	12.9	12.5	17.2	19.5	14.5	15.3	1.35 ± 0.79
	refined-I	11.7	10.5	13.4	12.3	13.6	12.3	1.06 ± 0.66
	refined-II	2.5	5.3	4.5	3.4	3.9	3.9	0.36 ± 0.19

^a Dipolar couplings originating on residues 1, 10–11, 24–26, 39–41, and 56 are excluded. ^b PDB entry 1IGD was used as the GB3 crystal structure.²³ For the refined-I structure, only C^α–C' and C'–N dipolar couplings were included in the refinement. Hydrogen atoms were placed at their standard positions (see text). For the refined-II structure, all dipolar couplings (C^α–C', C'–N, C^α–H^α and N–H) were used. ^c Q-factors reflect the agreement between structure and dipolar couplings: $Q = \text{rms}(D^{\text{calc}} - D^{\text{obs}}) / \{D_a^2[4 + 3R^2/5]\}^{1/2}$, where D_a and R refer to the magnitude and rhombicity of the alignment tensor, respectively, and D^{calc} and D^{obs} are the calculated and observed dipolar couplings, respectively. Subscripts A–E refer to the alignment medium used: A, bicelle; B, PEG; C, Pf1; phage; D and E, negatively and positively charged polyacrylamide gels, respectively. ^d Q_{av} refers to the average value over all five media. ^e Average rmsd per residue (compare second column of Table 3) between observed and predicted dipolar couplings. Values are normalized to a $D_a^{\text{N-H}}$ of 10 Hz.

restraints. The structure of refined-III with its H^N positions adjusted according to Table 3 and refined-IV with its H^α positions adjusted according to Supporting Information Table 5 have been deposited in the Protein Data Bank under accession numbers 1P7E and 1P7F, respectively.

Uncertainty in Alignment Tensor. The dipolar couplings obtained in one medium were randomly split into two equally sized subsets, and alignment tensor parameters were derived separately for each subset by singular value decomposition (SVD).^{41,42} Each subset has an error in alignment tensor parameters that is approximately $\sqrt{2}$ larger than that for parameters obtained from the whole set. Thus, the average pairwise rms deviation between cognate alignment tensor parameters equals twice the random error in the parameters obtained for a fit of the full data set. The SVD fits and error estimates were carried out using the crystal structure coordinates (1IGD)²³ as a reference.

Results and Discussion

Alignment of GB3 in Charged Polyacrylamide Gels. Compressed polyacrylamide gel is an attractive medium for aligning proteins relative to the magnetic field.^{18,19} Alignment within polyacrylamide gels is typically dominated by steric interactions and consequently yields similar average orientations

of the solute relative to the magnetic field as is obtained in liquid crystalline bicelle or PEG media.⁴³ In electrochromatography of biomolecules, polyacrylamide gels have been derivatized with charged compounds, offering the potential to introduce also an electrostatic component to the separation process. At present, electrostatically dominated alignment has been documented primarily for negatively charged media, including liquid crystalline solutions of Pf1 phage¹⁶ or cellulose particles⁴⁴ and purple membrane suspensions.^{41,45} Solute alignment in positively charged liquid crystalline media, including filamentous phage at low pH⁴⁶ and cetylpyridinium halide,^{47,48} has also been reported but is used less widely. The ability to modulate protein alignment by steric and attractive or repulsive electrostatic interactions is key to resolving the degeneracy that occurs when evaluating the dipolar couplings in terms of orientation.^{21,22} Here, we demonstrate that 2-acrylamido-2-methyl-1-propane-sulfonic acid (AMPS) and diallyldimethylammonium chloride (DADMAC) monomers are useful for introducing negative and positive charges, respectively, into the gel matrix and thus for altering the alignment tensor of GB3, used in the present study. A very recent report by Grzesiek and co-workers introduces negative charges by substitution of acrylic acid for acrylamide.⁴⁹

For GB3, a substantial change in alignment tensor was obtained by replacing 5% of the acrylamide (AA) monomers with an equimolar amount of AMPS. AA and AMPS are expected to polymerize at similar rates. However, DADMAC is known to polymerize at a much slower rate than AA.⁵⁰ The replacement of 5% AA with 10 times the equimolar amount of DADMAC yielded the desired change in alignment of GB3, which is negatively charged at our sample conditions (pI = 4.9). Compared to analogous gels with no or low amounts (<1%) of charged components, the alignment tensor magnitude for GB3 was about 45% higher in the presence of AMPS and about 40% higher in the presence of DADMAC, indicating substantial alignment contributions from electrostatic interaction. As an added benefit, it was found that, in contrast to regular gels, no shrinkage of the stretched gel in the NMR tube was observed over time, and the alignment magnitude of the protein in the NMR sample cell remained essentially constant over periods exceeding one month.

The similarity in the GB3 alignment tensors obtained in bicelle, PEG, Pf1, and the charged gel media is evaluated by calculating their normalized scalar products⁴¹ (Table 1). The low value of the scalar products obtained between the tensors in negatively charged gel and in the steric media (bicelles and PEG) indicates that the tensors differ substantially, and likewise the negatively charged Pf1 phage medium also differs substantially from the negatively charged gel. GB3 alignment in the positively charged gel appears to be relatively close to that in bicelles but differs considerably from that in PEG. The

(41) Sass, J.; Cordier, F.; Hoffmann, A.; Cousin, A.; Omichinski, J. G.; Lowen, H.; Grzesiek, S. *J. Am. Chem. Soc.* **1999**, *121*, 2047–2055.
 (42) Losonczi, J. A.; Andrec, M.; Fischer, M. W. F.; Prestegard, J. H. *J. Magn. Reson.* **1999**, *138*, 334–342.

(43) Ishii, Y.; Markus, M. A.; Tycko, R. *J. Biomol. NMR* **2001**, *21*, 141–151.
 (44) Fleming, K.; Gray, D.; Prasannan, S.; Matthews, S. *J. Am. Chem. Soc.* **2000**, *122*, 5224–5225.
 (45) Koenig, B. W.; Hu, J. S.; Ottiger, M.; Bose, S.; Hendler, R. W.; Bax, A. *J. Am. Chem. Soc.* **1999**, *121*, 1385–1386.
 (46) Barrientos, L. G.; Louis, J. M.; Gronenborn, A. M. *J. Magn. Reson.* **2001**, *149*, 154–158.
 (47) Prosser, R. S.; Losonczi, J. A.; Shiyonovskaya, I. V. *J. Am. Chem. Soc.* **1998**, *120*, 11010–11011.
 (48) Barrientos, L. G.; Dolan, C.; Gronenborn, A. M. *J. Biomol. NMR* **2000**, *16*, 329–337.
 (49) Meier, S.; Haussinger, D.; Grzesiek, S. *J. Biomol. NMR* **2002**, *24*, 351–356.
 (50) Brand, F.; Dautzenberg, H.; Jaeger, W.; Hahn, M. *Angew. Makromol. Chem.* **1997**, *248*, 41–71.

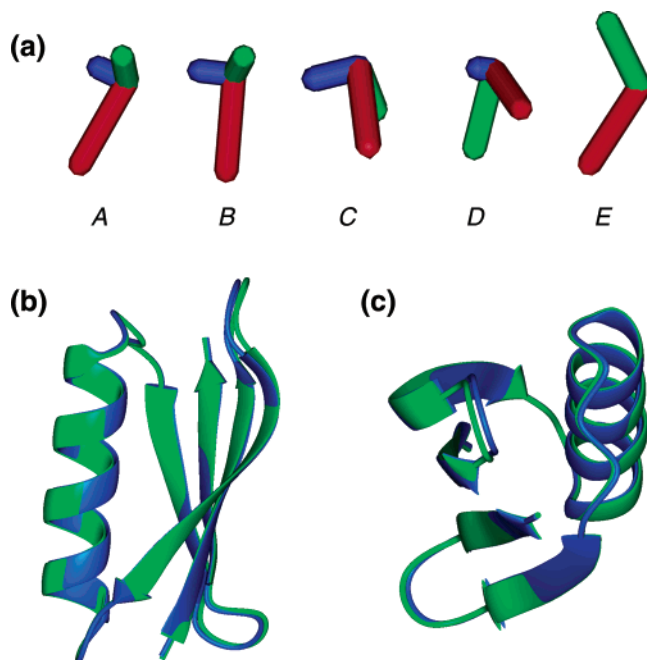


Figure 1. GB3 backbone ribbon diagrams and alignment tensors. (a) Orientation and magnitude of the alignment tensors obtained in media A–E (A, bicelle; B, PEG; C, Pf1 phage; D and E, negatively and positively charged polyacrylamide gels, respectively). The orientation of the principal alignment tensor frame relative to the GB3 orientation shown in (b) is depicted by the orthogonal axes systems shown. The length and orientation of the red, green, and blue axes correspond to the relative magnitude and sign of the alignment tensor components, D_{zz} , D_{yy} , and D_{xx} , respectively. Due to the high rhombicity of tensor E (0.66), its D_{xx} -axis is too short to be visible. (b,c) Ribbon representation of the GB3 crystal structure (blue), superimposed on the GB3 solution structure (refined-II; green). The C^α , C' , and N positions of both structures superimpose with a root-mean-square deviation of 0.32 Å.

orientations of the principal tensor frame in positively charged gel and in bicelles are quite similar (Figure 1a), but the tensor rhombicity of 0.66 is much larger in the gel than in bicelles (0.23). Overall, the relatively small values for the scalar products in Table 1 indicate that the five media offer valuable, complementary alignment information.⁴¹

GB3 Structure Refinement. Procedures that build hydrogen atoms to crystal structure coordinates and force fields used in the calculation of NMR structures generally place the backbone amide proton (H^N) on a line that bisects the $C'_i-N_{i+1}-C^\alpha_{i+1}$ angle, and the H^α proton is placed such that the $H^\alpha-C^\alpha$ vector makes equal tetrahedral angles of 109.4° with the $N-C^\alpha$ and $C^\alpha-C^\beta$ bonds.⁶ After energy minimization, these positions can change, depending on the specific geometric constraints used in the empirical energy function. For example, a commonly used parameter set in XPLOR moves H^N_{i+1} such that it falls in the $C^\alpha_i-C'_i-N_{i+1}$ plane. One of the aims of our present study is to evaluate which of these arrangements is optimal and whether small but systematic deviations exist. As uncertainties in heavy-atom positions translate into uncertainties in the H^N and H^α standard positions, it is prerequisite for this study that the positions of the backbone heavy atoms are known accurately. The availability of a 1.1 Å crystal structure for GB3 comes close to this requirement. However, when the agreement between observed and predicted $C^\alpha-C'$ and $C'-N$ dipolar couplings is assessed using this structure, differences that are significantly larger than the measurement error in the dipolar couplings are found (Table 2). Residual uncertainties in the crystal structure,

structural differences between the (average) solution and crystal structure, and internal protein dynamics are possible explanations for those differences. It is therefore desirable to first refine the crystal structure coordinates with the $C^\alpha-C'$ and $C'-N$ dipolar couplings. If the H^N and H^α protons are subsequently placed at their standard positions, the agreement between observed and calculated $C^\alpha-H^\alpha$ and $N-H$ dipolar couplings may be expected to improve somewhat upon use of the more accurate heavy-atom positions. Indeed, improvements are obtained for dipolar couplings observed in all five media (Table 2). Remarkably, if in turn the $C^\alpha-H^\alpha$ and $N-H$ dipolar couplings are also included in the refinement process, a small but statistically significant improvement in agreement between the experimental $C^\alpha-C'$ and $C'-N$ dipolar couplings and the calculated structure is observed (Table 2). While the $C^\alpha-C'$ and $C'-N$ dipolar couplings are included in both structure calculations, the addition of $C^\alpha-H^\alpha$ and $N-H$ dipolar coupling restraints improves the backbone structure slightly, as judged by improved agreement between measured and calculated $^1D_{C^\alpha C^\alpha}$ and $^1D_{C'N}$ couplings. This is remarkable because, in general, the addition of independent restraints makes it harder to fully satisfy the original restraints.

Very good agreement between measured and predicted dipolar couplings is observed for 46 out of 55 residues (Table 2), allowing identification of a nine-residue subset of residues that does not fit quite as well (albeit still reasonably well compared to what is typically found for other proteins). This subset includes K10-T11, E24-A26, V39-G41, and the C-terminal residue and was eliminated from the analysis below. For turn residues K10, T11, and V39-G41, the differences between observed and predicted couplings cannot be fully satisfied during the structure refinement, an indicator of pronounced internal dynamics.⁵¹ ^{15}N relaxation studies also indicate increased internal dynamics for these regions.⁵² Residues E24-A26 are located in GB3's α -helix and therefore are unlikely to be perturbed by large amplitude internal dynamics. However, measured backbone couplings for these residues are in considerably poorer agreement with those predicted from the X-ray structure than the remainder of the protein, presumably caused by rotameric averaging of several of their side chains, which has an effect on backbone geometry, but which is frozen out in the X-ray study, carried out at liquid N_2 temperature.

Figure 1 compares the original GB3 crystal structure with the new structure, refined as described above using a total of 984 $C^\alpha-C'$, $C'-N$, $C^\alpha-H^\alpha$, and $N-H$ dipolar coupling restraints, together with 34 hydrogen bond restraints, derived from $^3J_{NC'}$ couplings.³⁵ The two structures superimpose with a root-mean-square deviation (rmsd) of 0.32 Å on their C^α , C' , and N atom positions. The small changes in the β -sheet twist and the orientation of the turn connecting strands 2 and 3, observed in solution relative to the X-ray structure, are not surprising. Derrick and Wigley noted in their X-ray study that in the crystal, strand 2 of one monomer forms an antiparallel β/β interaction with strand 3 of the adjacent monomer, effectively forming a continuous plane of β -sheet throughout the crystal, thereby restraining the twist of the β -sheet.²³ Considering this, the difference between our solution structure and the crystal

(51) Meiler, J.; Prompers, J. J.; Peti, W.; Griesinger, C.; Bruschweiler, R. *J. Am. Chem. Soc.* **2001**, *123*, 6098–6107.

(52) Hall, J. B.; Fushman, D. *J. Biomol. NMR* **2003**, in press.

structure is remarkably small (Figure 1b,c). Interestingly, the crystal structure of GB3 in complex with its cognate Fab fragment (PDB entry 1IGC)²³ is closer to the solution structure of GB3 (refined-II; backbone rmsd = 0.51 Å) than the free GB3 crystal structure (1IGD; backbone rmsd 0.62 Å), in accordance with small global structural perturbations of free GB3 in its crystal environment. In particular, the slightly increased β -sheet twist observed in solution is similar to that seen in the X-ray structure of Fab-GB3 (data not shown). However, due to the much lower resolution of structure of the GB3-Fab complex (2.6 Å) compared to that of the isolated domain (1.1 Å), structural noise⁵³ is much higher for the complex, and consequently the dipolar coupling data fit relatively poorly to the complex.

Convergence of Dipolar Coupling Restraints. With the availability of five dipolar couplings per vector orientation, the question arises as to what extent a given N-H vector orientation can simultaneously satisfy all five experimental couplings.^{51,54,55} Each individual dipolar coupling, measured in a given alignment medium, restrains the orientation of the corresponding internuclear vector to the surface of a distorted cone about a principal axis of the alignment tensor.²¹ In a perfectly static description, and in the absence of measurement noise, all cones for a given N-H group would include the true vector orientation, which therefore must be located at the common intersection between the different cones. However, as pointed out previously,⁵¹ different degrees of dynamics for the various amides can result in the absence of a common intersection. Similarly, anisotropy of the internal N-H vector dynamics^{56–58} can cause this divergence from a common intersection, even if all N-H vectors exhibit identical internal dynamics.^{51,59} If the time- or ensemble-averaged orientation of a given N-H vector relative to the global molecular framework differs in the different alignment media, referred to as heterogeneous behavior, this also will result in the absence of a common intersection between cones.⁵⁵

The closer the pairwise intersection points of the five cones, derived for a given interaction vector by dipolar coupling measurement in five media, the smaller the effect of the above-mentioned factors. For GB3, we find that for the N-H vectors of all nonexcluded residues, the cones intersect one another to within the error in the $^1D_{\text{NH}}$ measurement and tensor magnitude, D_a . A representative subset of these is shown in Figure 2, for the backbone N-H orientations of residues N8, D22, F30, and G41. For N8, D22, and F30, a common intersection of the five cones is observed that agrees simultaneously with the five experimental $^1D_{\text{NH}}$ measurements, to within experimental error, whereas for G41 this is not the case. To express the proximity of the intersection points more quantitatively, the rmsd between experimental and predicted dipolar couplings is calculated as a function of N-H vector orientation. Minimal rms values, obtained at the point of closest intersection, of 0.28 Hz for N8, 0.17 Hz for D22, 0.31 Hz for F30, and 1.60 Hz for G41 are

Table 3. N-H Orientation in GB3, Yielding the Best Agreement with Experimental N-H Dipolar Couplings^a

residue ^b	rmsd (Hz) ^c	δ (deg) ^{a,d}	γ (deg) ^{a,d}
Y3	0.168	8.5 ± 1.5	-1.5 ± 1
K4	0.591	-3 ± 3	3 ± 3
L5	0.497	-2 ± 4	0 ± 0.5
V6	0.282	-1 ± 1	3 ± 1
I7	0.427	1 ± 2	1.5 ± 1
N8	0.279	5.5 ± 1.5	0 ± 0.5
G9	0.601	6 ± 3	2.5 ± 3
L12	0.864	3.5 ± 3	5.5 ± 1
K13	0.32	-11.5 ± 1.5	1.5 ± 1
G14	0.203	0.5 ± 1.5	0.5 ± 0.5
T16	0.376	1 ± 2.5	1 ± 4.5
T17	0.402	2.5 ± 3	1 ± 2.5
T18	0.233	-1 ± 2	2 ± 1.5
K19	0.847	-2 ± 4	-1 ± 1.5
A20	0.323	3.5 ± 1.5	0.5 ± 1
V21	0.307	-9.5 ± 1.5	-0.5 ± 1
D22	0.174	6 ± 2	1 ± 1
A23	0.722	-4.5 ± 3	1.5 ± 0.5
K28	0.213	0.5 ± 0.5	-0.5 ± 1
A29	0.222	4 ± 1	-0.5 ± 1
F30	0.305	-3 ± 1.5	2 ± 1
K31	0.258	-3.5 ± 1	1.5 ± 1
Q32	0.133	-4 ± 1	0 ± 0.5
Y33	0.297	0 ± 0.5	0.5 ± 1
A34	0.12	-3 ± 1	0.5 ± 0.5
D36	0.562	-4.5 ± 1	-0.5 ± 0.5
G38	0.259	-2.5 ± 2	2.5 ± 1
V42	0.253	-1 ± 1	-3.5 ± 2
W43	0.303	-8 ± 2.5	-3.5 ± 1.5
T44	0.356	0 ± 1.5	2 ± 1
D46	0.177	-1 ± 5.5	1 ± 4
D47	0.597	-5 ± 4.5	1.5 ± 2
A48	0.497	-3.5 ± 0.5	5.5 ± 1
T49	0.388	-7 ± 2	-1.5 ± 1
K50	0.631	-3 ± 1	5 ± 2
T51	0.156	5.5 ± 3.5	-4 ± 2.5
F52	0.512	9 ± 3.5	-2.5 ± 2
T53	0.211	-5.5 ± 1.5	1.5 ± 0.5
V54	0.313	1.5 ± 1.5	0 ± 1
T55	0.211	-1.5 ± 1	-2.5 ± 0.5

^a Orientation of the N-H bond is defined relative to the line bisecting the C'-N-C α angle by the in-plane rotation angle, γ , and the out-of-plane angle, δ (see Figure 4a). The GB3 crystal structure, refined with C α -C', C'-N, and C α -H α dipolar couplings (refined-III structure; cf. Supporting Information Table 3) is used as a reference. ^b Dipolar couplings originating on residues 10–11, 24–26, and 39–41 and on the N- and C-terminal residues are excluded. Due to spectral overlap, less than five N-H couplings could be obtained for residues Q2, E15, E27, N35, N37, and Y45, and these residues are also excluded. ^c All couplings were normalized to $D_a^{\text{NH}} = 10$ Hz for each medium. ^d Monte Carlo simulations (500), using Gaussian-distributed noise with a standard deviation of 0.26 Hz, were performed to estimate uncertainties.

found (when normalizing D_a^{NH} in each medium to 10 Hz). Averaged over all nonexcluded residues, a value of 0.36 ± 0.19 Hz is obtained (Table 3). An analogous analysis for the C α -H α dipolar couplings yields even better agreement, with an average rmsd of 0.45 ± 0.17 Hz (also normalized to $D_a^{\text{NH}} = 10$ Hz or $D_a^{\text{CH}} = 20.6$ Hz; Supporting Information Table 5). When the N-H and C α -H α couplings are included in the structure refinement process, in addition to the C α -C' and C'-N couplings, very similar average rmsd values are obtained: 0.36 ± 0.19 and 0.40 ± 0.19 Hz for $^1D_{\text{NH}}$ and $^1D_{\text{C}\alpha\text{H}\alpha}$, respectively (Table 2). This indicates that for the vast majority of residues (46 out of 55), a single structure simultaneously agrees with all five experimental dipolar couplings, and that with the exception of the above-noted excluded residues, there is no indication of large-amplitude internal motions or heterogeneous behavior in the different alignment media.

- (53) Zweckstetter, M.; Bax, A. *J. Biomol. NMR* **2002**, *23*, 127–137.
 (54) Peti, W.; Meiler, J.; Bruschweiler, R.; Griesinger, C. *J. Am. Chem. Soc.* **2002**, *124*, 5822–5833.
 (55) Hus, J. C.; Bruschweiler, R. *J. Biomol. NMR* **2002**, *24*, 123–132.
 (56) Fischer, M. W. F.; Zeng, L.; Pang, Y. X.; Hu, W. D.; Majumdar, A.; Zuiderweg, E. R. P. *J. Am. Chem. Soc.* **1997**, *119*, 12629–12642.
 (57) Lienin, S. F.; Bremi, T.; Brutscher, B.; Bruschweiler, R.; Ernst, R. R. *J. Am. Chem. Soc.* **1998**, *120*, 9870–9879.
 (58) Pang, Y. X.; Wang, L. C.; Pellecchia, M.; Kurochkin, A. V.; Zuiderweg, E. R. P. *J. Biomol. NMR* **1999**, *14*, 297–306.
 (59) Tolman, J. R.; Flanagan, J. M.; Kennedy, M. A.; Prestegard, J. H. *Nat. Struct. Biol.* **1997**, *4*, 292–297.

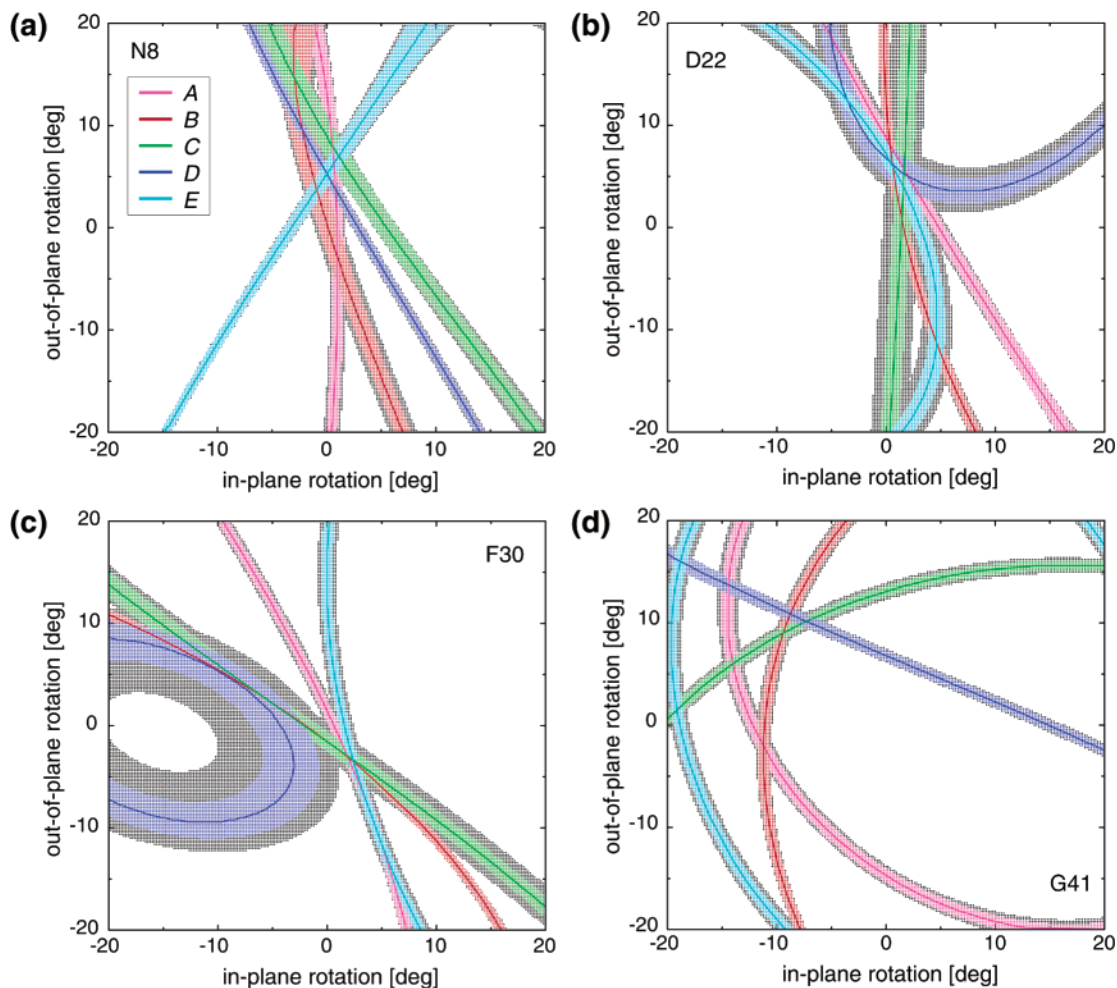


Figure 2. N–H vector orientations compatible with the measured $^1D_{\text{NH}}$ dipolar couplings of residue (a) N8, (b) D22, (c) F30, and (d) G41. Each colored “trajectory” of N–H vector orientations maps a small part of the intersection between a unit sphere and the cone of bond vector orientations, compatible with the experimentally measured coupling. Different colors correspond to the different aligning media, as marked in panel a and defined in the caption to Figure 1. The widths of the trajectories correspond to the experimental uncertainties in the measured $^1D_{\text{NH}}$ coupling and the alignment tensor (shown in gray). The alignment tensor used for each medium is the same as that used for the refinement of GB3 with inclusion of all $\text{C}^\alpha\text{--C}'$, $\text{C}'\text{--N}$, and $\text{C}^\alpha\text{--H}^\alpha$ couplings.

Dynamics of G41 and Upper Limit for Backbone Mobility.

For G41, the dipolar couplings in media A and E define N–H vector orientations that are not simultaneously compatible with those observed in media B–D (Figure 2d). The incompatibility of the N–H vector orientations defined by the five $^1D_{\text{NH}}$ dipolar couplings of G41, which is the most severe of all residues, could result either from increased or highly anisotropic internal dynamics^{51,54} or from a difference in the average structure of this flexible region in the different alignment media.⁵⁵ With an S^2 value of 0.5,⁵² G41 has been identified by ^{15}N relaxation as the most dynamic backbone amide in GB3. If internal motion were axially symmetric, the observed dipolar couplings would simply decrease by a factor S , which could be accounted for by uniformly increasing all five $^1D_{\text{NH}}$ dipolar couplings by a factor $1/S$. Indeed, for a scaling by 1.32, a minimal rmsd of 0.35 Hz is obtained (Figure 3a), which places G41 among the well-behaved GB3 residues and essentially corrects for its increased internal dynamics. This scale factor corresponds to a decrease in S^2 by a factor of 1.7 relative to the remainder of the backbone, in remarkable agreement with the recent ^{15}N relaxation study by Hall and Fushman.⁵² However, when all backbone amides are considered, scaling of the $^1D_{\text{NH}}$ couplings by their respective

$1/S$ values gives only a small (ca. 10%) improvement in the overall fit (Supporting Information Table 4). This indicates that, with the exception of residue G41, the inability to obtain a simultaneous fit to all five dipolar couplings appears not to be dominated by fast internal dynamics.

As pointed out by Meiler et al.,⁵¹ variations in S^2 along a protein’s backbone, which can also occur on a time scale slower than the rotational correlation time, generally make it impossible to obtain a perfect fit between dipolar couplings, measured in more than two linearly independent alignment media, and a single, static representation of the average structure. Here, we investigate the effect of random variations in S along the backbone of GB3 to estimate an upper limit for its variation over the entire range of time scales. Assuming cylindrically symmetric internal motion of an N–H vector about an average orientation, the observed dipolar coupling scales, to a very good approximation, by the generalized order parameter S .^{59–61} Starting from exact, back-calculated dipolar couplings, Monte Carlo simulations were carried out in which all five couplings

(60) Lipari, G.; Szabo, A. *J. Am. Chem. Soc.* **1982**, *104*, 4546–4559.

(61) Tjandra, N.; Omichinski, J. G.; Gronenborn, A. M.; Clore, G. M.; Bax, A. *Nat. Struct. Biol.* **1997**, *4*, 732–738.

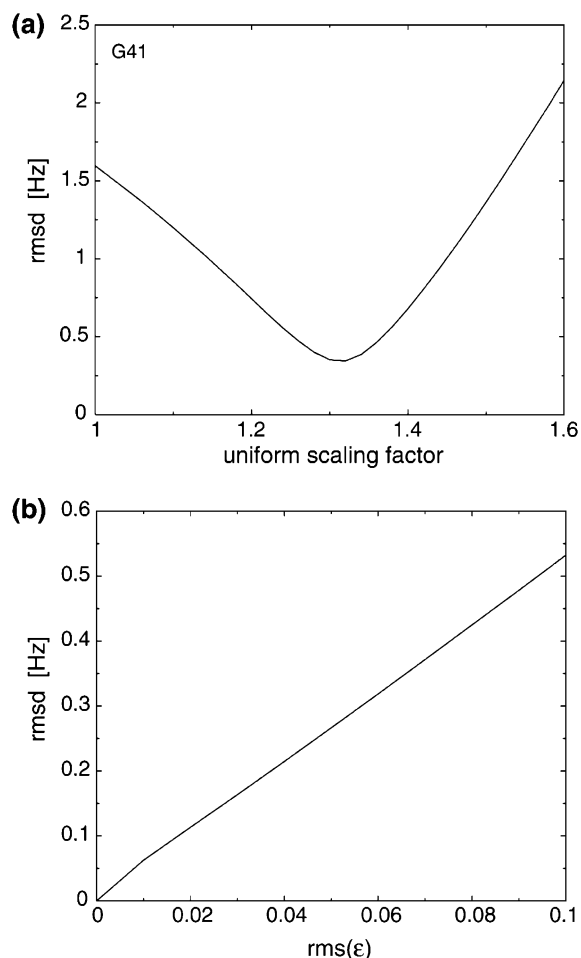


Figure 3. Dependence of dipolar fit quality on internal dynamics. (a) Minimal rmsd between the five experimental $^1D_{\text{NH}}$ dipolar couplings of G41 and the values calculated for a single, static orientation, as a function of the uniform scaling factor of the five dipolar couplings. (b) Simulated effect of variation in internal dynamics along GB3's backbone. For each residue, n , the five $^1D_{\text{NH}}$ dipolar couplings per residue, back-calculated from the X-ray crystal structure, are scaled by $1 + \epsilon_n$, followed by finding the N–H orientation that best fits the scaled dipolar couplings. The plotted curve represents the average rmsd between the randomly scaled, simulated dipolar couplings and the corresponding values for the N–H orientation that best fits simultaneously to these scaled values. The horizontal axis corresponds to the rms value of ϵ_n , with ϵ Gaussian-distributed around zero. Reported values are averaged over 500 simulations.

for any given amide, n , are multiplied by a factor $1 + \epsilon_n$. The value of ϵ_n is a random number selected from a Gaussian distribution centered about zero and simulates the random variations in S . Subsequently, the N–H vector orientation is optimized to minimize the rmsd between all five modified dipolar couplings for each N–H. Figure 3b shows that the residual error in the fit of the $^1D_{\text{NH}}$ values increases approximately linearly with the rms value of ϵ . The lowest rmsd obtained for a single, static structure and the observed backbone $^1D_{\text{NH}}$ couplings for the well-ordered regions of the backbone is on average 0.36 Hz (Table 2). This slightly exceeds the estimated random rms error in the measurement of 0.26 Hz, and it is likely that this higher rmsd results, at least in part, from dynamic effects. An upper limit for the degree of variation in S^2 along the backbone is obtained if all of the discrepancy is assigned to dynamic effects (i.e., assuming zero measurement error). For $\text{rms}(\epsilon) = 0.068$, the error in the fit equals the average rmsd (0.36 Hz) observed for the experimental data, and this

$\text{rms}(\epsilon)$ value therefore provides an upper limit for the variation in S . A better estimate of the variability in S also considers the experimental error in $^1D_{\text{NH}}$ (0.26 Hz). Assuming this experimental error and variation in S to be uncorrelated, the variation in S only contributes $(0.36^2 - 0.26^2)^{1/2} = 0.25$ Hz to the inability to fit the experimental dipolar couplings perfectly to a static structure. The graph of Figure 3b indicates that this corresponds to an rms variation of $\pm 4.7\%$ in values of S . This rms is likely to represent an overestimate of its true variation, as the error in the $^1D_{\text{NH}}$ measurement was determined from evaluating the reproducibility of the measurement, not accounting for any possible small systematic errors. Moreover, this analysis also ignores errors in the magnitude of the alignment tensors, which would also increase the error in the fit.

Amide Proton Position. The tight definition of N–H vector orientations by the obtained dipolar couplings permits evaluation of the deviation of the amide proton from its standard position, i.e., from the line that bisects the $C'_i\text{--}N_{i+1}\text{--}C^{\alpha}_{i+1}$ angle (Figure 4a). Considering that these deviations are small, they may simply be expressed by two rotation angles: γ , describing the required rotation in the peptide plane, and δ for the rotation out of the $C'_i\text{--}N_{i+1}\text{--}C^{\alpha}_{i+1}$ plane (Figure 4a). For $\delta \ll \pi/2$, δ is related to the angle θ_N between the planes defined by $C'\text{NH}$ and $C'\text{NC}^{\alpha}$ by $\delta = \theta_N/\sin(\zeta)$, where ζ is the angle between the $C'\text{--}N$ and $N\text{--}H$ bonds. As mentioned previously, the γ and δ angles at which the rmsd between the five predicted and measured $^1D_{\text{NH}}$ couplings is minimal represent the best measure for the average orientation of an N–H vector. The contour plots of the rmsd as a function of N–H vector orientation show well-defined minima (Figure 4d and Supporting Information Figure 1) and Table 3 summarizes the obtained rotation angles at the point of minimal rms deviation. Figure 4b shows that the deviation from the standard position, averaged over all residues, is very small ($\langle\gamma\rangle = 0.7^\circ$; $\langle\delta\rangle = -0.8^\circ$), but interestingly, the out-of-plane variation relative to the mean ($\text{rms } \delta = 4.7^\circ$) is about 2-fold larger than the in-plane variation ($\text{rms } \gamma = 2.3^\circ$). For α -helical amides, a slightly larger average out-of-plane deviation is seen ($\langle\gamma\rangle = 0.5^\circ$; $\langle\delta\rangle = -2.0^\circ$; Figure 4c), with less variation ($\text{rms } \gamma = 1.0^\circ$; $\text{rms } \delta = 3.4^\circ$) than observed in the remainder of the protein. For β -sheet amides, the average orientation coincides perfectly with the standard orientation ($\langle\gamma\rangle = 0.0^\circ$; $\langle\delta\rangle = -0.1^\circ$), but the degree of variation is larger than that for α -helical amides ($\text{rms } \gamma = 2.1^\circ$; $\text{rms } \delta = 4.8^\circ$). For the remaining residues, outside regions of secondary structure, the variation is largest ($\text{rms } \gamma = 3.2^\circ$; $\text{rms } \delta = 5.4^\circ$) with average amide positions of $\langle\gamma\rangle = 2.2^\circ$ and $\langle\delta\rangle = -1.2^\circ$.

As discussed above, even after refinement against the dipolar couplings, the backbone C and N coordinates still contain small random errors. Therefore, the above listed γ and δ angles include random contributions resulting from these errors, increasing their spread. However, considering that these backbone coordinate errors are random, they contribute a similar degree of randomness to the in-plane, γ , and out-of-plane, δ , angles. The much larger residue-to-residue variation in δ than in γ therefore indicates that, at least for δ , the above found variations are dominated by true deviations of the N–H vector from its standard orientation.

N Pyramidalization Contributes to Nonplanarity of Peptide Bond. The question of whether deviations from peptide bond planarity result from a true twist about the $C'\text{--}N$ bond or

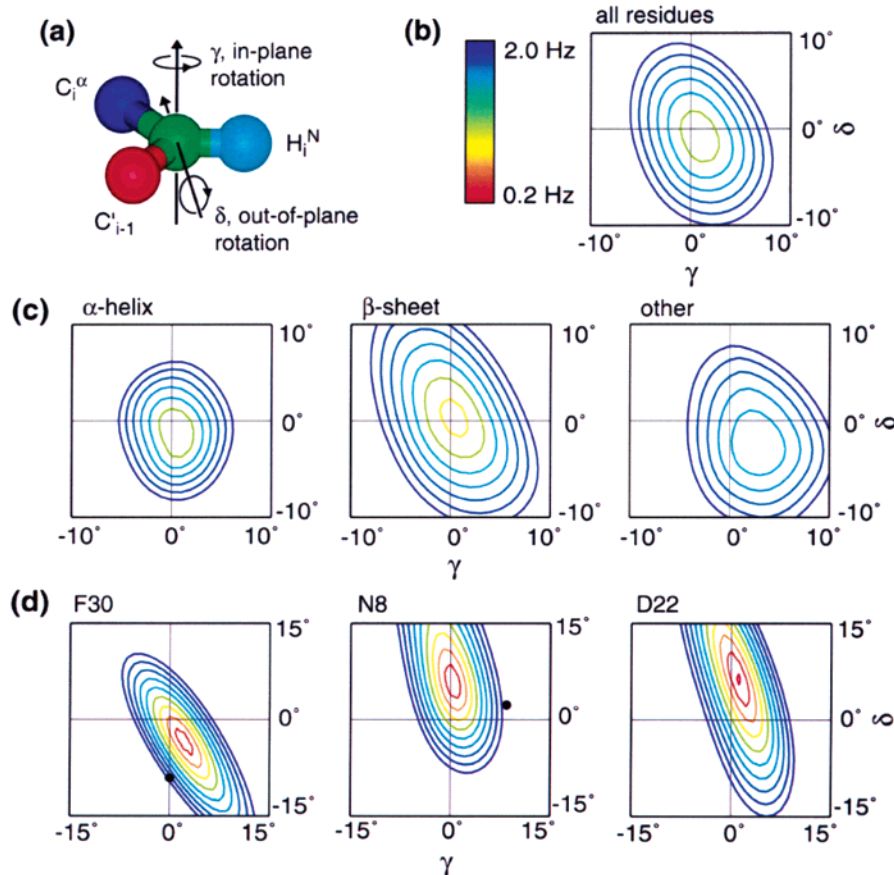


Figure 4. Deviation of the N–H bond orientation from its standard orientation along the line bisecting the C'_i – N_{i+1} – C^{α}_{i+1} angle. (a) Definition of the sign of the in-plane (γ) and out-of-plane (δ) rotation angles relative to the idealized planar geometry. Both γ and δ rotation axes were chosen orthogonal to the standard N–H orientation. (b) Contour plot of the rmsd between observed and predicted $^1D_{\text{NH}}$ dipolar couplings as a function of uniform rotations of all N–H vectors away from their standard orientation, averaged over all nonexcluded residues. Values are normalized to a D_{a}^{NH} of 10 Hz. Ten contour levels ranging from 0.2 to 2 Hz in steps of 0.2 Hz are used and color-coded as depicted. (c) Contour plots analogous to those in b, but with the amides separated by type of secondary structure (9 residues in α -helix, 21 in β -sheet, 10 in “other”). (d) Contour plots analogous to those in b for three individual residues, N8, D22, and F30, belonging to the secondary structure classes shown in (c). The corresponding full set is shown as Supporting Information. For H^{N} nuclei forming intramolecular hydrogen bonds, the orientation of the vector between the N and H-bond accepting O is marked by a solid black dot.

from pyramidalization of the N has been the subject of considerable debate.^{62,63} A pure twist would leave the N_{i+1} – H_{i+1} vector in the C'_i – N_{i+1} – C^{α}_{i+1} plane, whereas in the absence of twist, N pyramidalization results in a C^{α}_i – C'_i – N_{i+1} – C^{α}_{i+1} torsional angle, ω_i , that exactly supplements the C^{α}_i – C'_i – N_{i+1} – H_{i+1} torsion angle, Ω_i (i.e., $\Omega_i + \omega_i = 180^\circ$). A plot of the experimentally determined out of C'_i – N_{i+1} – C^{α}_{i+1} plane angles, δ_{i+1} , versus ($\omega_i - 180^\circ$) for the backbone amides in GB3 is shown in Figure 5. A weak correlation is observed ($R = -0.52$), with a slope of approximately -1 and a small offset of -2° . The correlation's slope of -1 indicates that, on average, about half of the peptide bond twist observed in GB3 results from pyramidalization, and half represents a true twist about the C' – N bond. However, the large degree of scatter in the correlation indicates that this rule does not apply to each residue, but only to the average.

The correlation between ω_i and the out of C'_i – N_{i+1} – C^{α}_{i+1} plane angle, δ_{i+1} , suggests that, in the absence of an abundance of dipolar couplings defining the peptide bond, it is best to position the amide proton such that the C^{α}_i – C'_i – N_{i+1} – H_{i+1}

torsion angle is -2° , rather than in the C'_i – N_{i+1} – C^{α}_{i+1} plane. The in-plane orientation, γ_{i+1} , appears to be independent of ω_i (data not shown), and the standard definition in which the C'_i – N_{i+1} – H_{i+1} and C^{α}_{i+1} – N_{i+1} – H_{i+1} angles have identical values remains optimal. For example, if hydrogens are added to the GB3 backbone N atoms using this new protocol instead of placing them on the C'_i – N_{i+1} – C^{α}_{i+1} bisector, the rmsd between the out-of-plane angle δ (Table 3) and the out-of-plane angle of the corresponding modeled position is reduced from 4.7 to 3.9° . Concomitantly, a slight improvement (3–8%, depending on which GB3 backbone structure is used) of the fit to the experimental $^1D_{\text{NH}}$ values is observed.

Our data are in good qualitative agreement with earlier work. In a crystallographic study of cyclic lactams, Winkler and Dunitz found that pyramidalization of the backbone N contributes about as much to deviations from $\omega = 180^\circ$ as does pure twisting of the C' – N bond.⁶⁴ A more recent analysis by MacArthur and Thornton of very high-resolution crystal structures of small peptides in the Cambridge Structural Database found, averaged over 650 residues, a δ/ω correlation that is qualitatively similar to that of Figure 5.⁸ These authors also noted a systematic difference in the out-of-plane angle, δ , for right-handed versus left-handed chain direction. Although not contradicted by our

(62) Ramachandran, G. N.; Lakshminarayanan, A. V.; Kolaskar, A. S. *Biochim. Biophys. Acta* **1973**, *303*, 8–13.

(63) Burton, N. A.; Chiu, S. S. L.; Davidson, M. M.; Green, D. V. S.; Hillier, I. H.; McDouall, J. J. W.; Vincent, M. A. *J. Chem. Soc., Faraday Trans.* **1993**, *89*, 2631–2635.

(64) Winkler, F. K.; Dunitz, J. D. *J. Mol. Biol.* **1971**, *59*, 169–182.

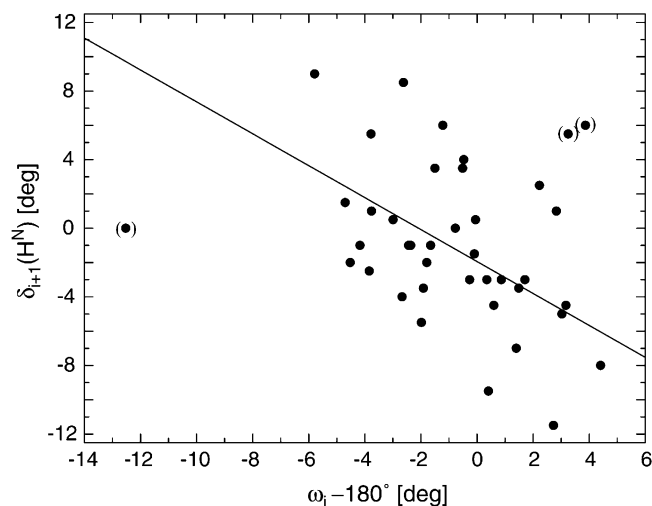


Figure 5. Plot of the out-of- $C'_i-N_{i+1}-C^{\alpha}_{i+1}$ plane angle, δ_{i+1} , of the amide N–H vector, as a function of the $C^{\alpha}_{i-1}-C'_i-N_{i+1}-C^{\alpha}_{i+1}$ torsion angle, ω_i . The ω angles are taken from the refined-III structure, calculated by including $C^{\alpha}-C'$, $C'-N$, and $C^{\alpha}-H^{\alpha}$ dipolar couplings, and the N–H vector orientation relative to this backbone that yields best agreement with the five $^{15}\text{N}-^1\text{H}$ dipolar couplings is used for deriving δ values (Table 3). The three apparent outliers, marked by brackets, are excluded from the linear fit $\delta_{i+1} = -0.93(\omega_i - 180^\circ) - 2.0^\circ$. The correlation coefficient, R , is -0.52 .

data, at the large degree of scatter in our δ/ω correlation, this systematic difference was not statistically significant. The small 2° offset in our correlation (Figure 5) was also noted by MacArthur and Thornton, but only for chain regions with a left-handed twist (for which $\phi + \psi > 0$).

It might be expected that N–H vector orientations also correlate with the position of the H-bond accepting carbonyl oxygen relative the H-bond donating amide. For amides where the N–O vector falls within the $\pm 15^\circ$ window of Figure 4d and Supporting Information Figure 1, the direction of the N–O vector is also marked, but no correlation between the N–O vector orientation and the N–H deviation from its standard orientation was discernible, even when including H-bond accepting oxygens outside the window shown. Apparently, the effect of the H-bond accepting oxygen on the N–H bond vector orientation is small and masked by other parameters, such as the backbone torsion angles ϕ and ψ , and steric interactions that are a function of the side chain torsion angles. The observation, noted above, that the average out-of-plane orientation varies little with secondary structure argues against a simple ϕ/ψ dependence, but the small number of residues available in each type of secondary structure makes it impossible to discern whether χ_1 -dependent steric interactions are modulated by the backbone torsion angles.

Asymmetric Motion of the N–H Vector. Molecular dynamics simulations of internal motions in proteins suggest that fluctuations of N_i-H_i bond vector orientations are larger for motions in the plane orthogonal to the $C^{\alpha}_{i-1}-C^{\alpha}_i$ vector than for those within the $C^{\alpha}_{i-1}-N_i-C^{\alpha}_i$ plane.⁶⁵ In particular, so-called crank-shaft motions, with opposite-signed fluctuations in ψ_{i-1} and ϕ_i , can contribute considerably to the anisotropy of backbone amide internal motion.⁶⁶ NMR relaxation parameters, both for backbone ^{15}N autorelaxation⁵⁷ and $^{13}\text{C}'$ -related cross-relaxation rates,⁵⁶ confirm this anisotropy in internal dynamics,

but the degree of anisotropy remains a matter of debate. Here we address this question on the basis of the observed dipolar N–H couplings.

Assuming uniformity along the backbone in the amplitude and anisotropy of the internal N–H bond vector dynamics, the effect of anisotropic internal motion on the observed dipolar couplings can be separated into a uniform scaling, which accounts for the fraction of motion that is cylindrically symmetric in amplitude with respect to the average N–H vector orientation, and a distribution of out-of-plane orientations for this average N–H vector orientation. Cylindrically symmetric internal motion of limited amplitude simply results in a uniform scaling of the dipolar couplings and is therefore of no concern. The width of the orientational distribution of N–H vectors out of the $C^{\alpha}_{i-1}-N-C^{\alpha}_i$ plane reflects how much larger fluctuations are out-of-plane than in-plane.

A total of 200 $^1D_{\text{NH}}$ dipolar couplings (40 residues in five media) were calculated for ensembles of GB3 structures, with the N–H vectors uniformly distributed, in 1° increments, across an arc in the plane orthogonal to the $C^{\alpha}_{i-1}-C^{\alpha}_i$ axis. The rmsd between the average of the calculated $^1D_{\text{NH}}$ couplings and the corresponding observed coupling is evaluated as a function of the width of the N–H distribution. Figure 6a demonstrates that if the X-ray structure, refined by inclusion of $C^{\alpha}-C'$, $C^{\alpha}-H^{\alpha}$, and $N-C'$ couplings (refined-III; Supporting Information Table 3), is used as a reference structure, a very shallow minimum is observed for an angular distribution spanning $\pm 6^\circ$. However, the increase in rmsd for larger out-of-plane motions does not become statistically significant until the width of this distribution exceeds $\pm 17^\circ$. The shallowness of the minimum observed in Figure 6a results from the weak dependence of the dipolar couplings on small amplitude motions about an average and also from the relatively high starting value of the rmsd in the absence of any asymmetry in internal motion. As discussed above, this “starting value of the rmsd” results, at least in part, from the assumption that the N–H vector is located on the line bisecting the $C'-N-C^{\alpha}$ angle. If starting N–H orientations are used that agree best with all four types of dipolar couplings (Table 2, refined-II), including $^1D_{\text{NH}}$, the initial rmsd is much lower, and the agreement between observed and calculated dipolar couplings decreases significantly when the amplitude of the out-of-plane distribution exceeds $\pm 10^\circ$ (Figure 6b).

For comparison, the same calculations can be performed when using an ensemble with the N–H bond vector distributed on an arc within the $C^{\alpha}_{i-1}-N_i-C^{\alpha}_i$ plane, as would apply in the case where in-plane N–H motions were larger than out-of-plane. For both starting models, the agreement between calculated and observed dipolar couplings decreases more rapidly as a function of distribution width for the in-plane case than for an out-of-plane distribution (Figure 6).

H^{α} Proton Position. In analogy to the analysis conducted for the H^{N} nuclei, deviations of the $C^{\alpha}-H^{\alpha}$ vector from its standard orientation have been examined. Commonly, the $C^{\alpha}-H^{\alpha}$ bond vector is model-built such that it makes equal, ideal tetrahedral angles of 109.4° with the $C^{\alpha}-N$ and $C^{\alpha}-C'$ bonds.⁶ Deviations in the $C^{\alpha}-H^{\alpha}$ vector orientation are again expressed as a function of two rotation angles, γ (toward C^{β}) and δ (to the $C^{\alpha}-H^{\alpha}-C^{\beta}$ plane), as depicted in Figure 7a. The obtained rotation angles at the point of minimal rmsd between all five $C^{\alpha}-H^{\alpha}$ dipolar coupling restraints are summarized in Supporting

(65) Breml, T.; Bruschiweiler, R. *J. Am. Chem. Soc.* **1997**, *119*, 6672–6673.

(66) Fadel, A. R.; Jin, D. Q.; Montelione, G. T.; Levy, R. M. *J. Biomol. NMR* **1995**, *6*, 221–226.

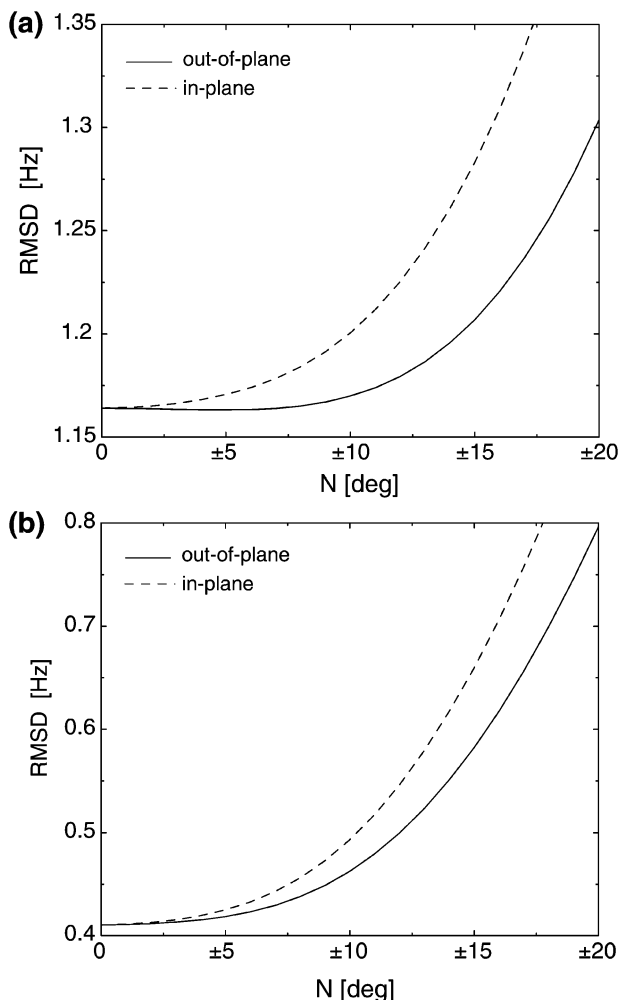


Figure 6. Plots of the rmsd between 200 $^1D_{\text{NH}}$ values, measured in five alignment media, and corresponding values calculated for ensembles of structures. The ensembles consist of $2N + 1$ structures, with all the amide N–H vectors rotated in 1° steps about the $\text{C}^\alpha\text{--C}^{\alpha+1}$ direction, such as to cover out-of-plane arcs of $\pm N$ degrees relative to their starting position (solid line), or $\pm N$ degree in-plane arcs (dashed line) by rotation about an axis orthogonal to the peptide plane. The starting structures were the refined-III structure (Supporting Information Table 3) with (a) the N–H vectors at their standard position (Figure 4a) and (b) the N–H vectors at their optimal positions (Table 3). When the $^1D_{\text{NH}}$ values for the ensembles of structures were calculated, the alignment tensor was fixed at the values used for deriving the refined-III structure.

Information Table 5. With the exception of D46 for which the minimum is very shallow, individual $\text{C}^\alpha\text{--H}^\alpha$ orientations are again well defined (Figure 7d and Supporting Information Figure 2). Extreme deviations ($>10^\circ$) are found for V42 and T55, possibly indicative of dynamics or small errors in the local structure, and these residues are excluded in the following discussion.

The deviation in the $\text{C}^\alpha\text{--H}^\alpha$ orientations from their idealized tetrahedral orientations, averaged over all residues, is again very small ($\langle\gamma\rangle = -0.7^\circ$; $\langle\delta\rangle = -0.6^\circ$; Figure 7b). The rms variations are 3.0° for γ and 2.3° for δ , which is more symmetric and of somewhat smaller amplitude than for the N–H case. When solely considering α -helical residues, a small deviation from the standard orientation is evident ($\langle\gamma\rangle = -1.8 \pm 2.7^\circ$; $\langle\delta\rangle = -1.6 \pm 2.7^\circ$; Figure 7c). For β -sheet residues, the average γ and δ values are close to zero ($\langle\gamma\rangle = -0.3 \pm 2.3^\circ$ and $\langle\delta\rangle = -0.2 \pm 2.6^\circ$). Outside regions of regular secondary structure,

the average γ and δ values are very close to zero, but the degree of variation in γ appears to be larger ($\langle\gamma\rangle = -0.3 \pm 4.2^\circ$; $\langle\delta\rangle = -0.3 \pm 2.1^\circ$). However, the possibility that a larger uncertainty in local backbone structure is partly responsible for this small increase in γ variability cannot be excluded.

No correlation between γ or δ values and either residue type or χ_1 angle could be detected. Therefore, although considerable deviations from 109.4° are known to occur for the τ_3 angle¹³ ($\tau_3 = 109.4 \pm 2.9^\circ$ for the 1IGD X-ray structure, $109.9 \pm 2.4^\circ$ for the refined-II structure), the commonly used assumption of equal 109.4° $\text{H}^\alpha\text{--C}^\alpha\text{--C}^\beta$ and $\text{H}^\alpha\text{--C}^\alpha\text{--N}$ angles⁶ appears to be near optimal when adding H^α coordinates to an X-ray structure.

Concluding Remarks

The availability of an atomic resolution X-ray crystal structure for GB3 and the ability to measure an extensive set of backbone dipolar couplings in five different media allow exploration of a wide range of questions.

First, our study demonstrates that refinement of a very high-resolution crystal structure by inclusion of experimental dipolar couplings for $\text{C}^\alpha\text{--C}'$ and $\text{N--C}'$ increases the agreement between observed N–H or $\text{C}^\alpha\text{--H}^\alpha$ dipolar couplings and values predicted from the structure. This indicates that even for the highest resolution crystal structures, agreement between the dipolar couplings and structure is not limited by intrinsic dynamic behavior of the protein.

Second, our data indicate that the commonly used assumption, that the N–H vector is located on the line bisecting the $\text{C}'\text{--N--C}^\alpha$ angle, is close to optimal for all types of secondary structures. However, our data also show that pyramidalization at the N position does occur, and the rms out-of-plane angle in GB3 was found to be 4.7° , with a maximum value of $11.5 \pm 1.5^\circ$ for K13. These out-of-plane values are very similar to those previously reported for a 1 Å structure of BPTI ($\langle\delta\rangle = 0.4 \pm 4.8^\circ$), jointly refined using X-ray and neutron diffraction data (PDB entry 5PTI).⁷ However, the systematic rotation of the N–H vector toward the N– C^α bond ($\langle\gamma\rangle = 3.5 \pm 3.9^\circ$), seen in the BPTI structure, is much less pronounced in the GB3 structure. The weak correlation observed in our data between the out-of-plane angle, δ , and the $\text{C}^\alpha\text{--C}'\text{--N}_{i+1}\text{--C}^{\alpha+1}$ torsion angle, ω , indicates that on average, pyramidalization contributes comparably to the deviation from peptide bond planarity as does true twisting about the $\text{C}'\text{--N}$ bond, in good agreement with earlier work.⁶⁴ In all cases, pyramidalization at the N position is much smaller than that seen in theoretical calculations of model compounds. This discrepancy is likely to result from an increase in double-bond character in protein peptide bonds, caused by hydrogen bonding of both the NH and CO moieties. Pyramidalization at the N position has opposite effects on the $\text{C}^\alpha\text{--C}'\text{--N}_{i+1}\text{--C}^{\alpha+1}$ and $\text{C}^\alpha\text{--C}'\text{--N}_{i+1}\text{--H}_{i+1}$ torsion angles, and our finding that approximately half of the variation in $\text{C}^\alpha\text{--C}'\text{--N}_{i+1}\text{--C}^{\alpha+1}$ torsion angle results from pyramidalization points to a slightly improved method for adding H^{N} protons to crystal structures, by fixing the $\text{C}^\alpha\text{--C}'\text{--N}_{i+1}\text{--H}_{i+1}$ torsion angle at -2° . This average deviation from a planar arrangement has been noted previously and attributed to the chirality of amino acids and the handedness of the chain direction.⁸

Third, for the vast majority of GB3 residues, a very good fit, which approaches the experimental uncertainty, could be

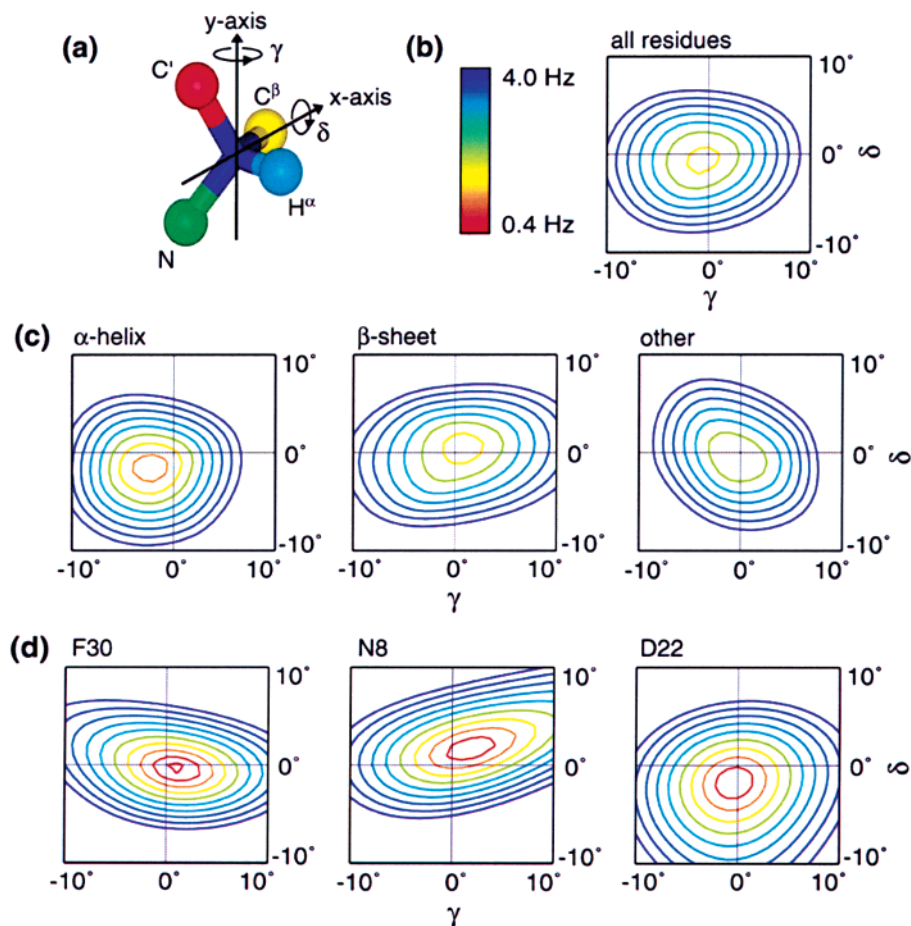


Figure 7. Deviation of the C α -H α bond vector from its standard orientation, defined as the line that makes 109.4° angles with the N-C α and C α -C β bonds. (a) Definition of the x- and y-axes, orthogonal to the C α -H α bond, about which rotations by angles δ and γ are carried out. The x-axis is chosen in the C β -C α -H α plane; the y-axis is orthogonal to x and C α -H α . (b) Contour plot of the rmsd between observed and predicted $^1D_{C\alpha H\alpha}$ dipolar couplings as a function of uniform rotations of all C α -H α vectors away from their standard orientation, averaged over all nonexcluded residues. Values are normalized to a $D_a^{C\alpha H\alpha}$ of 20.6 Hz (corresponding to a D_a^{NH} of 10 Hz). Ten contour levels ranging from 0.4 to 4 Hz in steps of 0.4 Hz are used and color-coded as indicated. (c) Contour plots analogous to those in b, but with the C α sites separated by type of secondary structure (11 residues in α -helix, 20 in β -sheet, and 9 in "other"). (d) Contour plots analogous to those in b for three individual residues, F30, N8, and D22, belonging to the secondary structure classes shown in c. The corresponding full set is available as Supporting Information.

obtained between the static structure and experimental dipolar couplings. This differs from what has been found previously for protein structures of lower crystallographic resolution,^{54,59} where differential dynamics along the peptide backbone had been suggested as the cause of the poor fit. If the discrepancy between observed dipolar couplings and optimized static N-H orientations in GB3 is entirely attributed to variation in backbone dynamics, Monte Carlo simulations indicate that $\pm 6.8\%$ variation in the backbone order parameter, S , is needed to explain the discrepancy. This indicates that the amplitude of internal dynamics along GB3's backbone is far more homogeneous than previously seen in other proteins. On the other hand, for a small subset of GB3 residues, no simultaneous agreement between dipolar couplings measured in five media and a single static structure can be obtained, indicative of internal dynamics.⁵¹ For residue G41, for example, which previously has been identified as the most dynamic backbone amide in GB3, we find that simply scaling all five $^1D_{NH}$ dipolar couplings observed for this amide by a uniform factor of 1.32 results in agreement between structure and this coupling to within experimental error. This indicates that for this residue, the simplest isotropic wobbling-in-a-cone model can satisfactorily restore agreement between the time-averaged dipolar coupling and a static structure.

Fourth, our data are consistent with, but do not prove, the commonly accepted Gaussian Axial Fluctuation (GAF) model where internal dynamics of the N-H vector in the plane orthogonal to the C α_{i-1} -C α_i axis are of larger amplitude than motions in the C α_{i-1} -N $_i$ -C α_i plane.^{57,65} However, our data also indicate that the amplitude of the out-of-plane fluctuations does not exceed that of the in-plane motions by more than 10–15°, in agreement with dynamics simulations.⁶⁵

Finally, even though considerable variation exists in the N-C α -C' angle (τ_3), our data indicate that the commonly used approximation, which places the C α -H α vector such that it makes ideal tetrahedral H α -C α -C β and H α -C α -N angles, is near optimal and that residue-to-residue deviations from this orientation are small.

Acknowledgment. We thank Elena Gustchina for preparing isotopically labeled GB3 and Marius Clore and David Bryce for many useful suggestions. T.S.U. is supported by a Long-Term Fellowship from the Human Frontier Science Program.

Supporting Information Available: Figure with contour plots of the root-mean-square deviation between experimental and predicted N-H couplings as a function of N-H vector

orientation for all residues (except the excluded ones); an analogous figure for the $C^\alpha-H^\alpha$ dipolar couplings; table giving the force constants used in the structure refinement of GB3; table with the GB3 alignment tensor parameters obtained in media A–E; table with Q factors for the crystal and refined GB3 structures; table with the root-mean-square deviation between D_{NH} values observed in five media and the value predicted for the orientation that yields the best simultaneous

agreement with these five couplings, in the absence and presence of S scaling; table with the γ and δ values that yield optimal agreement between dipolar couplings and $C^\alpha-H^\alpha$ vector orientation; table containing the experimental dipolar couplings in media A–E. This material is available free of charge via the Internet at <http://pubs.acs.org>.

JA0350684